

Sub-millimetre observations of hyperluminous infrared galaxies

D. Farrah¹, S. Serjeant², A. Efstathiou³, M. Rowan-Robinson¹, A. Verma⁴

¹*Astrophysics Group, Blackett Laboratory, Imperial College, Prince Consort Road, London SW7 2BW, UK*

²*Unit for Space Sciences & Astrophysics, School of Physical Sciences, University of Kent at Canterbury, Canterbury, Kent, CT2 7NZ, UK*

³*Department of Computer Science and Engineering, Cyprus College, 6 Diogenous Street, PO Box 22006, 1516 Nicosia, Cyprus*

⁴*Max-Planck-Institut für Extraterrestrische Physik, Postfach 1312, 85741 Garching, Germany*

Received 2001 October 31

ABSTRACT

We present sub-mm photometry for 11 Hyperluminous Infrared Galaxies (HLIRGs, $L_{IR} > 10^{13.0} h_{65}^{-2} L_{\odot}$) and use radiative transfer models for starbursts and AGN to examine the nature of the IR emission. In all the sources both a starburst and AGN are required to explain the total IR emission. The mean starburst fraction is 35%, with a range spanning 80% starburst dominated to 80% AGN dominated. In all cases the starburst dominates at rest-frame wavelengths longwards of $50\mu\text{m}$, with star formation rates $> 500 M_{\odot}\text{yr}^{-1}$. The trend of increasing AGN fraction with increasing IR luminosity observed in IRAS galaxies is observed to peak in the HLIRG population, and not increase beyond the fraction seen in the brightest ULIRGs. The AGN and starburst luminosities correlate, suggesting that a common physical factor, plausibly the dust masses, govern the luminosities of starbursts and AGN in HLIRGs. Our results suggest that the HLIRG population is comprised both of ULIRG-like galaxy mergers, and of young galaxies going through their maximal star formation periods whilst harbouring an AGN. The detection of coeval AGN and starburst activity in our sources implies that starburst and AGN activity, and the peak starburst and AGN luminosities, can be coeval in active galaxies generally. When extrapolated to high- z our sources have comparable observed frame sub-mm fluxes to sub-mm survey sources. At least some high- z sub-mm survey sources are therefore likely to be comprised of similar galaxy populations to those found in the HLIRG population. It is also plausible from these results that high- z sub-mm sources harbour heavily obscured AGN. The differences in X-ray and sub-mm properties between HLIRGs at $z \sim 1$ and sub-mm sources at ~ 3 implies some level of evolution between the two epochs. Either the mean AGN obscuration level is greater at $z \sim 3$ than at $z \sim 1$, or the fraction of IR-luminous sources at $z \sim 3$ that contain AGN is smaller than that at $z \sim 1$.

Key words: infrared: galaxies – galaxies: active – galaxies: Seyfert – galaxies: starburst – Quasars: general

1 INTRODUCTION

One of the most important results from the Infrared Astronomical Satellite (*IRAS*) all sky surveys was the detection of a new class of galaxy where the bulk of the bolometric emission lies in the infrared waveband (Soifer et al. 1984; Sanders & Mirabel 1996). This population, termed ‘Luminous Infrared Galaxies’ (LIGs), becomes the dominant extragalactic population at IR luminosities above $10^{11} L_{\odot}$, with a higher space density than all other classes of galaxy of comparable bolometric luminosity.

At the brightest end of the LIG population lie the Hyperluminous Infrared Galaxies (HLIRGs), those with $L_{IR} > 10^{13.0} h_{65}^{-2} L_{\odot}$ (Rowan-Robinson 2000). The first HLIRG to be found (P09104+4109) was identified by Kleinmann et al. (1988), with a far infrared luminosity of $1.5 \times 10^{13} h_{50}^{-2} L_{\odot}$. In 1991, Rowan-Robinson et al. identified F10214+4724 at $z = 2.286$, with an apparent far infrared luminosity of $3 \times 10^{14} h_{50}^{-2} L_{\odot}$. Later observations of this object revealed a huge mass of molecular gas ($10^{11} h_{50}^{-2} M_{\odot}$ (Brown & vanden Bout 1991; Solomon, Downes & Radford 1992)), a Seyfert

emission spectrum (Elston et al. 1994), high optical polarisation (Lawrence et al. 1993), and evidence for lensing with a magnification of about 10 at infrared wavelengths (Graham & Liu 1995; Broadhurst & Lehar 1995; Eisenhardt et al. 1996; Green & Rowan-Robinson 1996). These objects appeared to presage an entirely new class of infrared galaxy.

The source and trigger of the IR emission in HLIRGs is currently the subject of considerable debate. HLIRGs may simply be the high luminosity tail of the ULIRG population, where mergers between evolved galaxies trigger dust shrouded starburst and AGN activity (Sanders & Mirabel 1996). There is evidence from *HST* observations (Farrah et al. 2002) that at least some HLIRGs are merging galaxies. A second possibility is that HLIRGs may be very young, or ‘primeval’ galaxies. Rowan-Robinson (2000) argues that the majority of the emission at rest-wavelengths $> 50\mu\text{m}$ in HLIRGs is due to starburst activity, implying star formation rates $> 1000M_{\odot}\text{yr}^{-1}$. If the rest-frame far infrared and sub-mm emission from HLIRGs is due to star formation, then the star formation rates would be the highest for any objects in the Universe. This would strongly suggest these galaxies are going through their maximal star formation periods, implying that they are galaxies in the first stages of formation. A final possibility is that the IR emission arises via some other mechanism (e.g. a transient IR luminous phase in QSO evolution not triggered by interactions), HLIRGs would then be an entirely different class of object.

In this paper we study the infrared emission from HLIRGs using data from the optical to the sub-mm. We present new sub-mm data for a sample of 11 HLIRGs, and use radiative transfer models for starbursts and AGN, in conjunction with previously published IR photometry, to examine the power source behind the IR emission. Sample selection, observations and data analysis are described in §2. The radiative transfer models used to evaluate the IR emission are described in §3. Results are presented in §4, and notes on individual sources are given in §5. Discussion is presented in §6 and conclusions are summarized in §7. We have taken $H_0 = 65 \text{ km s}^{-1} \text{ Mpc}^{-1}$, $\Omega = 1.0$ and $\Omega_{\Lambda} = 0.0$.

2 THE SAMPLE

2.1 Sample Selection and Observations

The objects in our sample are taken from the FIR selected sample presented by Rowan-Robinson (2000). Unlike nearly all previous studies of HLIRGs, the sample in our study is selected in a manner independent of obscuration, inclination or AGN content. Together with the statistical homogeneity and completeness of the parent samples, our sample is therefore entirely free from AGN bias and suitable for drawing global conclusions about the HLIRG population.

Observations were made using the Submillimetre Common User Bolometer Array (SCUBA, Holland et al. 1999) on the James Clerk Maxwell Telescope (JCMT) on October 11-12 2000 and on January 8-17 2001. SCUBA contains two bolometer arrays, one containing 37 pixels and optimized for observations at $850\mu\text{m}$, and the other containing 91 pixels and optimized for observations at $450\mu\text{m}$. In most circumstances, both arrays are operated simultaneously using a dichroic. Observations were performed using SCUBA’s

photometry mode, in which data is taken using only a single pixel on each array. For each integration the secondary mirror was jiggled so that the selected bolometer in each array sampled a 3×3 grid with $2''$ spacing between grid positions, centred on the source. During each integration the secondary mirror is chopped by $45''$ in azimuth with a frequency of 7Hz in order to remove sky variations. After each integration, the telescope is then nodded to a reference position $45''$ away in azimuth to remove hotspots in the internal SCUBA optics. Each object was observed for approximately 40 minutes, depending on weather conditions. Sky opacities during the observations were of moderate quality, with measured opacities at 225GHz from the Caltech Submillimetre Observatory (CSO) in the range $0.075 < \tau_{225} < 0.15$. Calibration observations were made of Mars or Uranus, or of a secondary calibrator if no primary calibrator was available. Skydips were taken before and after each object and calibrator observation.

2.2 Data Reduction

The SCUBA User Reduction Facility (SURF) software was used to reduce the data for all objects. The data were first flatfielded and despiked. Atmospheric extinction corrections at $450\mu\text{m}$ and $850\mu\text{m}$ were derived by extrapolating from the CSO τ_{225} extinction values following the prescription of Archibald, Wagg & Jenness (2000). These extrapolated values were checked for consistency against the observed $450\mu\text{m}$ and $850\mu\text{m}$ extinctions from the skydips. Residual sky gradients not removed by nodding and chopping were removed by averaging over all the bolometers in each array, and subtracting this value from the measured source flux. Individual integrations for each source were then concatenated into a single exposure. Each concatenated dataset was checked for internal consistency using a Kolmogorov-Smirnov (K-S) test. Finally, flux calibration for each source was carried out using the FLUXES package together with the calibrators listed in Table 1. In those cases where the calibrator has a larger spatial extent than the 9 point photometry mode jigglemap the flux of the calibrator in a single photometry jigglemap was used to calibrate the sources, rather than the total flux of the calibrator.

3 INFRARED EMISSION MODELS

3.1 Starburst Models

To model the IR emission due to starburst activity we used the starburst models of Efsthathiou, Rowan-Robinson & Siebenmorgen (2000). These models consider an ensemble of evolving HII regions containing hot young stars, embedded within Giant Molecular Clouds (GMCs) of gas and dust. The composition of the dust is given by the dust grain model of Siebenmorgen & Krugel (1992), which includes Polycyclic Aromatic Hydrocarbons. The stellar populations within the GMCs evolve according to the stellar synthesis codes of Bruzual & Charlot (1993). The star formation rate is assumed to decay exponentially with an e-folding timescale of 2×10^7 years. The models vary in starburst age from zero years up to 7.2×10^7 years, with 11 discrete values.

Table 1. Hyperluminous Galaxies observed by SCUBA

Name	RA (J2000) hh:mm:ss	Dec ° ' "	z	Type ¹	Obs. Date	Calibrator
IRAS F00235+1024	00 26 06.7	10 41 27.6	0.58	nl	October 2000	Uranus
IRAS 07380-2342	07 40 09.8	-23 49 57.9	0.29	nl	January 2001	oh 231
IRAS F10026+4949	10 05 52.5	49 34 47.8	1.12	Sy1	January 2001	oh 231
IRAS F12509+3122	12 53 17.6	31 05 50.5	0.78	QSO	January 2001	Mars
IRAS 13279+3401	13 30 15.3	33 46 28.7	0.36	QSO	January 2001	Mars
IRAS 14026+4341	14 04 38.8	43 27 07.2	0.32	Sy1	January 2001	Mars
IRAS F14218+3845	14 23 55.5	38 31 51.3	1.21	QSO	January 2001	Mars
IRAS F16124+3241	16 14 22.1	32 34 03.7	0.71	nl	January 2001	Mars
ELAISP90 J164010+410502	16 40 10.2	41 05 22.1	1.10	QSO	January 2001	Mars
IRAS 18216+6418	18 21 57.3	64 20 36.4	0.30	Sy1	October 2000	Uranus
IRAS F23569-0341	23 59 33.6	-03 25 12.8	0.59	nl	October 2000	Uranus

Positions and redshifts are taken from the NASA Extragalactic Database. ¹Spectral Type, taken from Rowan-Robinson 2000 & NED. 'nl' - Narrow Line object, 'Sy1' - Seyfert 1.

3.2 AGN Torus Models

To model the IR emission due to AGN, we used the AGN models of Efstathiou & Rowan-Robinson (1995). These models incorporate accurate solutions to the axially symmetric radiative-transfer problem in dust clouds to model the IR emission from dust in active galactic nuclei. Dust composition is given by the multigrain dust model of Rowan-Robinson (1992). We have used the thick tapered disk models following an r^{-1} density distribution, as this subset of models has been found to be most successful in satisfying the observational constraints of AGN. The AGN models vary in torus opening angle from 0° to 90° , with 15 discrete values.

4 RESULTS

4.1 Spectral Energy Distributions

We combined our measured sub-mm fluxes and 3σ upper limits with optical and IR data from the literature to fit Spectral Energy Distributions (SEDs) for each object. For each source we obtained *IRAS* fluxes and 3σ upper limits from the Faint Source Catalogues (Moshir et al. 1992), or by using the SCANPI v5.0 software. Where available, we obtained *B* and *R* band magnitudes from the APM catalogues, and near-IR fluxes from the 2MASS catalogues. Additional photometry for each source is described in section 6. The compiled fluxes for each object are given in Table 2.

Emission from unobscured population II and III stars is not included in either the starburst or AGN models, and care must be taken in accounting for this. For example, a recent *HST* study of ULIRGs (Farrah et al. 2001) found that the optical emission was in most cases dominated by old stellar populations and not by light from a starburst or AGN. To avoid the uncertainties in assuming an arbitrary SED for an evolved stellar population, we have assumed that all emission shortwards of $4\mu\text{m}$ in the rest frame of the objects contains a significant but unquantified contribution from old stellar populations. As this contribution could lie between 0% and 100%, any measured flux at a rest-frame wavelength shorter than $4\mu\text{m}$ is treated as a 3σ upper limit in the fitting, unless the contribution from the host galaxy has been previously removed.

Goodness of fit was examined by using the reduced χ^2 statistic. Fits for all sources were good, with $\chi_{best}^2 \leq 1.5$ in all cases. To determine the errors on the luminosities and model parameters we explored χ^2 space between χ_{best}^2 and $\chi_{best}^2 + 2$. The SEDs for those sources with sufficient IR photometry to constrain the shape of the SED are given in Figure 1. The total IR luminosities for each source, the starburst and AGN components, and the best fit model parameters are given in Table 3.

There exist models for the IR emission from dusty QSOs (Rowan-Robinson 1995) where the dust can extend several hundred parsecs from the nucleus instead of the several tens of parsecs found in other AGN models (Efstathiou & Rowan-Robinson 1995). The dust at these large radii will have a temperature of 20 - 70 Kelvin, as opposed to the dust several tens of parsecs from the AGN, which will have a temperature of a few hundred Kelvin. If extended dust around an AGN were present in any of our sample the sub-mm emission from this dust could be mistakenly ascribed to star formation, thus overestimating the star formation rates. To test this, we fitted the models of Rowan-Robinson (1995) to the objects in our sample, both on their own and in combination with the starburst models described previously. In all cases the extended AGN dust models were clearly rejected by the fitting. We therefore conclude that sub-mm emission from extended dust surrounding an AGN is not viable for the objects in our sample.

4.2 Star Formation Rates

Estimating obscured star formation rates from IR data is based on silicate and graphite dust grains absorbing the optical and UV light from young stars and reradiating in the IR and sub-mm. A recent estimate for deriving star formation rates from IR luminosities has been made by Rowan-Robinson et al. (1997):

$$\dot{M}_{*,all} = 2.6 \times 10^{-10} \frac{\phi L_{60}}{\epsilon L_{\odot}} \quad (1)$$

where $\dot{M}_{*,all}$ is the rate of formation of stars, ϵ is the fraction of optical/UV light from the starburst that is absorbed by the dust and re-emitted in the IR, and L_{60} is the $60\mu\text{m}$

Table 2. Compiled Photometry from the optical to the sub-mm for the HLIRGs in our sample

Name	S_I	S_J	S_H	S_K	$S_{6.7}$	S_{12}	S_{25}	S_{60}	S_{100}	S_{450}	S_{850}
F00235+1024 ^a	0.08	–	–	–	0.92 ± 0.38	< 173	< 193	428 ± 55.6	< 938	< 967	< 6.38
07380-2342 ^b	1.11	–	–	–	–	484 ± 28	801 ± 80	1170 ± 88	3546 ± 280	< 1275	26.8 ± 4.2
F10026+4949	0.04	–	–	–	–	< 86	177 ± 35	266 ± 30	310 ± 80	< 386	< 7.91
F12509+3122 ^c	0.86	0.96	0.81	1.13	–	< 106	103 ± 26	218 ± 44	309 ± 82	< 333	< 9.23
13279+3401 ^d	–	–	–	–	–	< 94	< 126	1182 ± 77	1196 ± 165	< 274	< 9.22
14026+4341 ^e	–	3.36	4.76	8.19	–	118 ± 27.1	285 ± 29	622 ± 57.0	994 ± 239	< 94	< 7.53
F14218+3845 ^f	0.05	–	–	–	0.79 ± 0.26	< 96.9	< 74.9	< 565	< 2100	< 253	< 8.55
F16124+3241 ^g	–	–	–	0.15	–	< 65	< 55	174 ± 35	290 ± 90	< 103	8.47 ± 2.2
E J1640+41 ^h	–	0.44	0.63	0.56	4.99 ± 0.66	< 102	< 57	< 81	< 336	< 82	< 6.97
18216+6418 ⁱ	–	8.8	13.0	22.1	109 ± 11	211 ± 14	395 ± 45	1128 ± 113	2159 ± 252	< 308	14.8 ± 2.6

All fluxes are given in mJy. Unless stated in the text, all fluxes at rest-frame wavelengths shortward of 4 μ m are treated as upper limits in the SED fitting, due to the unquantified contribution from the host galaxy. Sources for additional photometry are described in §6. Additional photometry: (a) $S_{15} = 6.752 \pm 2.143$, $S_{90} = 477.9 \pm 147.9$, $S_{180} = 804.7 \pm 393.3$ (b) $S_B = 0.062$, $S_R = 0.346$ (c) $S_B = 1.41$, $S_V = 0.751$, $S_R = 0.72$ (d) $S_B = 0.50$, $S_R = 2.38$ (e) $S_B = 3.23$, $S_R = 5.48$, $S_{4.0} = 16$, $S_{7.0} = 36 \pm 4$ (f) $S_B = 0.06$, $S_R = 0.114$, $S_{15} = 3.228 \pm 1.036$, $S_{90} = 163.5 \pm 61$, $S_{180} = < 1765$ (g) $S_B = 0.014$, $S_R = 0.079$ (h) $S_{15} = 7.75 \pm 0.72$, $S_{90} = 72 \pm 23$ (i) $S_U = 9.04$, $S_B = 8.12$, $S_V = 7.55$, $S_L = 60.5$, $S_{9.63} = 143 \pm 14.3$, $S_{1100} = < 47$, $S_{1250} = < 3.7$

starburst luminosity. The factor ϕ incorporates the correction between a Salpeter IMF and the true IMF ($\times 1.0$ for a Salpeter IMF, $\times 3.3$ for a Miller-Scalo IMF), and also a correction for the assumed upper and lower stellar mass bounds for the stars forming in the starburst ($\times 1.0$ if the mass range is $0.1 < M_\odot < 100$, $\times 0.323$ if the mass range is assumed to form only OBA type stars, i.e. $1.6 < M_\odot < 100$). We have assumed that all of the optical/UV light from the starburst is absorbed ($\epsilon \sim 1.0$), and that the IMF of the starburst is a Salpeter IMF forming stars across the mass range $0.1 < M_\odot < 100$, ($\phi = 1.0$). The calculated star formation rates for our sample using Equation 1 are given in Table 3.

4.3 Dust Masses and Temperatures

Dust temperatures cannot be directly determined from the starburst or AGN models described in sections 3.1 and 3.2, as these models do not assume an isothermal temperature distribution. Monolithic dust temperatures, although unphysical simplifications in AGN, can serve as a useful comparison with previous work. Dust temperature estimates were calculated by fitting an optically thin greybody function of the form:

$$S_\nu = \nu^\beta B(\nu, T_{dust}) \quad (2)$$

to the FIR SED over the wavelength range 200 – 1000 μ m. In Equation 2 S_ν is the source flux at a frequency ν , T_{dust} is the dust temperature, $B(\nu, T_{dust})$ is the Planck function, and β is the frequency dependence of the grain emissivity.

Gas and dust masses can be estimated directly from the starburst models. The total mass of Giant Molecular Clouds (GMC's, which include both gas and dust) is straightforward to estimate, as stars are assumed to form from the GMC's. The mass of stars at time t^* can be written:

$$M_s(t^*) = \eta M_{GMC}(t^*) = \int_0^{t^*} \dot{M}_s(t) dt \quad (3)$$

where $M_{GMC}(t^*)$ is the mass of Giant Molecular Clouds at time t^* , $\dot{M}_s(t)$ is the star formation rate and η is the efficiency of conversion of GMC's to stars. Approximating the

star formation rate as an exponential decay with a characteristic e-folding time of $\tau = 20$ Myr (ERS 00), then it is trivial to show that:

$$M_{GMC}(t^*) = \frac{\tau \dot{M}_s(t^*)}{\eta} \left[\frac{1}{e^{-\frac{t^*}{\tau}} - 1} \right] \quad (4)$$

where M_{GMC} is given in multiples of $10^6 M_\odot$ as τ is given in multiples of 10^6 years. This however gives the total mass of GMCs in the system at the current age of the starburst, without accounting for the effects of supernovae winds, which will remove some fraction of gas and dust from the system either via photodestruction of dust grains or by blowing the gas and dust out of the starburst regions. Estimates using Equation 4 may therefore significantly overestimate the gas and dust masses in the system, unless the starburst is very young. For the purposes of this analysis it is better to estimate dust masses directly from the sub-mm SED. An approach for estimating dust and gas masses in galaxies using sub-mm data is to assume the system is optically thin at these wavelengths, and to follow the prescription of Hildebrand (1983):

$$M_{dust} = \frac{1}{1+z} \frac{S_{\nu_o} D_L^2}{\kappa(\nu_r) B(\nu_r, T_{dust})} \quad (5)$$

where ν_o and ν_r are the observed and rest frame frequencies respectively, S_{ν_o} is the flux in the observed frame, $B(\nu_r, T_{dust})$ is the Planck function in the rest frame and T_{dust} is the dust temperature. The gas mass is then obtained by assuming a fixed gas to dust ratio. For the most extreme *IRAS* galaxies, the best current estimate of the gas to dust ratio is 540 ± 290 (Sanders, Scoville & Soifer 1991). For comparison, the gas to dust ratio in spiral galaxies is thought to be ~ 500 (Devereux & Young 1990), and ~ 700 in ellipticals (Wiklind & Henkel 1995). The mass absorption coefficient in the rest frame, κ_r , is taken to be:

$$\kappa_r = 0.067 \left(\frac{\nu_r}{2.5 \times 10^{11}} \right)^\beta \quad (6)$$

in units of $\text{m}^2 \text{kg}^{-1}$ and the luminosity distance is assumed to be of the form:

$$D_L = \frac{c}{H_0 q_0^2} (q_0 z + (q_0 - 1) [(2q_0 z + 1)^{\frac{1}{2}} - 1]) \quad (7)$$

Dust masses and temperatures for our sample calculated using Equations 2 and 5 are given in Table 3.

4.4 Individual Sources

4.4.1 IRAS F00235+1024

This narrow line object is not detected in the X-ray to a limit of $L_X/L_{bol} = 2.3 \times 10^{-4}$, indicating either atypically weak X-ray emission or an obscuring column of $N_H > 10^{23} \text{cm}^{-2}$ (Wilman et al. 1998). *HST* imaging (Farrah et al. 2002) shows an interacting object, with no optical QSO. *ISO* observations (Verma et al. 2002) imply that the IR emission is dominated ($> 60\%$) by a starburst, but that an AGN contribution is required to explain the MIR emission.

The best fit SED model for this object is given in Figure 1. Additional *I* band data was taken from Farrah et al. (2002), and additional *ISO* fluxes were compiled from Verma et al. (2002). The SED of this object is best explained by a combination of starburst and AGN components. The *ISO* detections at $6.7\mu\text{m}$ and $15\mu\text{m}$ combined with the sub-mm upper limits make it impossible to fit this source with a pure starburst. We find that the AGN and starburst components contribute comparably to the total IR emission. The starburst component dominates at wavelengths $> 60\mu\text{m}$. The best fit model parameters are a dust temperature of 35 Kelvin, a dust mass of $1.95 \times 10^8 M_\odot$, a star formation rate of $\sim 1000 M_\odot \text{yr}^{-1}$, and a line of sight angle to the AGN torus of $< 17.2^\circ$. The strong mid-IR absorption feature at $15\mu\text{m}$ predicted by the combined SED fit results from viewing an AGN dust torus almost edge on through intervening absorption by cooler dust.

4.4.2 IRAS 07380-2342

The best fit SED model for this object is given in Figure 1. Additional *I* band data was taken from archival *HST* observations. This narrow line HLIRG is best fitted by a combination of starburst and AGN components where the AGN component dominates overall ($\sim 65\%$), but where the starburst dominates at wavelengths longward of $45\mu\text{m}$. The IR data is best fit by a young (6.6 - 16Myr) starburst with a star formation rate of $1250 M_\odot \text{yr}^{-1}$, and an AGN component with a line of sight angle of $< 20^\circ$. The dust temperature and mass are 31K and $6.6 \times 10^8 M_\odot$ respectively.

4.4.3 IRAS F10026+4949

HST imaging of this source (Farrah et al. 2002) shows moderate morphological disturbance and multiple very close companions. The object is thus assumed to be in ongoing interactions. We compiled additional *I* band data for this object from Farrah et al. (2002). With only three fluxes, there exists insufficient IR photometry to model the IR SED. The fluxes combined with the upper limits do however allow constraints to be drawn on both the total IR luminosity, and the starburst and AGN components. The best fit predicts a total IR luminosity of $\sim 6.5 \times 10^{13} L_\odot$, with the AGN providing $\sim 80\%$ of the total IR emission. The star formation rate is extremely high, at $\sim 2000 M_\odot \text{yr}^{-1}$.

4.4.4 IRAS F12509+3122

This QSO shows no signs of interaction, and has an undisturbed bright elliptical host (Farrah et al. 2002). We obtained additional *I* band data from Farrah et al. (2002), which is treated as a flux rather than an upper limit in the SED fitting as the host galaxy magnitude is known. The best fit to the IR SED predicts a total IR luminosity of $\sim 1.82 \times 10^{13} L_\odot$, where the AGN component provides the majority ($\sim 60\%$) of the emission over the whole SED but where the starburst dominates at wavelengths $> 50\mu\text{m}$. The dust temperature and emissivity are 39K and 1.94 respectively, with a predicted star formation rate of $\sim 1050 M_\odot \text{yr}^{-1}$. An SED fit is plotted in Figure 1. The model slightly underpredicts the *I* band flux. This is likely due to treating the other optical fluxes as upper limits. As this object is a QSO the optical emission will arise mostly from the AGN, and indeed the host galaxy contribution in the *I* band is very small (Farrah et al. 2002). For consistency with the other sources we have treated the other optical fluxes as upper limits, as trial fits show that fitting to the optical points as fluxes makes no difference to the derived IR luminosities.

4.4.5 IRAS 13279+3401

This broad line object has only two measured fluxes, so constraints can only be drawn on the total IR luminosity, and the best fit AGN and starburst components. The best fit predicts a total IR luminosity of $\sim 8.7 \times 10^{12} L_\odot$ with the AGN component providing the majority ($\sim 70\%$) of the emission.

4.4.6 IRAS 14026+4341

This radio quiet BAL QSO was discovered by Low et al. (1989). *HST* imaging shows that the host is a luminous elliptical, and that the host is involved in ongoing interactions (Hutchings & Morris 1995). Optical spectropolarimetry (Hines et al. 2001) shows that the polarized flux density is dependent on wavelength, indicating that the polarization is produced by dust scattering.

The best fit SED for this object is presented in Figure 1. For this object we obtained additional unpublished *ISO* photometry (Belinda Wilkes, priv. comm.). The best fit model predicts a total IR luminosity of $7.9 \times 10^{12} L_\odot$ with the AGN component providing $\sim 60\%$ of the IR emission. The derived dust temperature and mass are 35K and $1.7 \times 10^8 M_\odot$ respectively, with a star formation rate of $\sim 600 M_\odot \text{yr}^{-1}$.

4.4.7 IRAS F14218+3845

This QSO possesses a small very luminous host with no signs of ongoing interactions and an undetermined morphology (Farrah et al. 2002). *ISO* observations (Verma et al. 2002) suggest that the IR emission is best explained as being predominantly (74%) starburst in origin, but with the AGN component dominating at wavelengths $< 30\mu\text{m}$.

Additional *ISO* photometry was compiled from Verma et al. (2002), and additional *I* band data from Farrah et al. (2002). The *I* band data is treated as a flux rather than an upper limit as the host galaxy magnitude is known. The best fit predicts a total IR luminosity of $1.15 \times 10^{13} L_\odot$. The

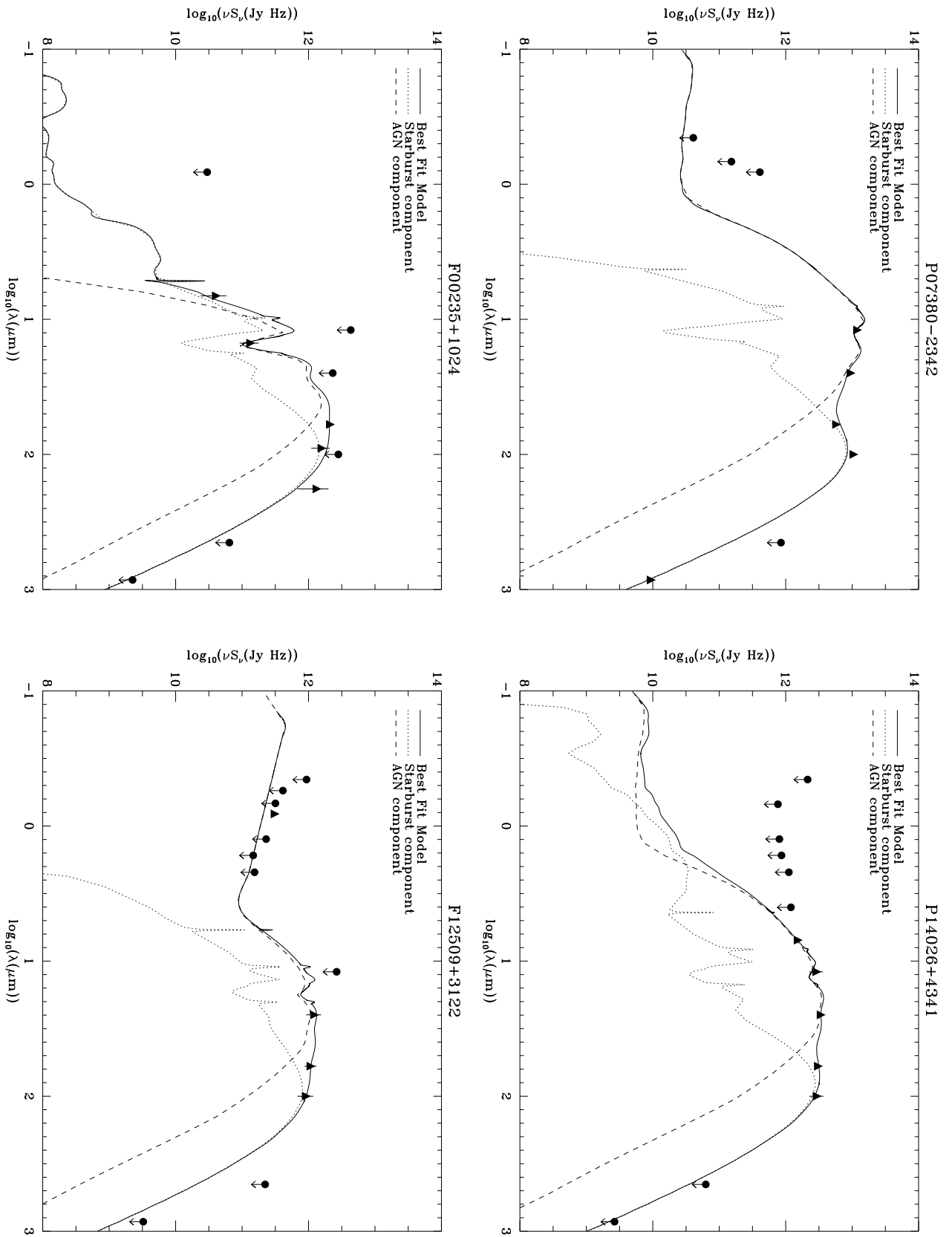


Figure 1. Best fit combined models in the observed frame, and the AGN and Starburst components, for F00235+1024, 07380-2342, F12509+3122, 14026+4341, F14218+3845 & 18216+6418

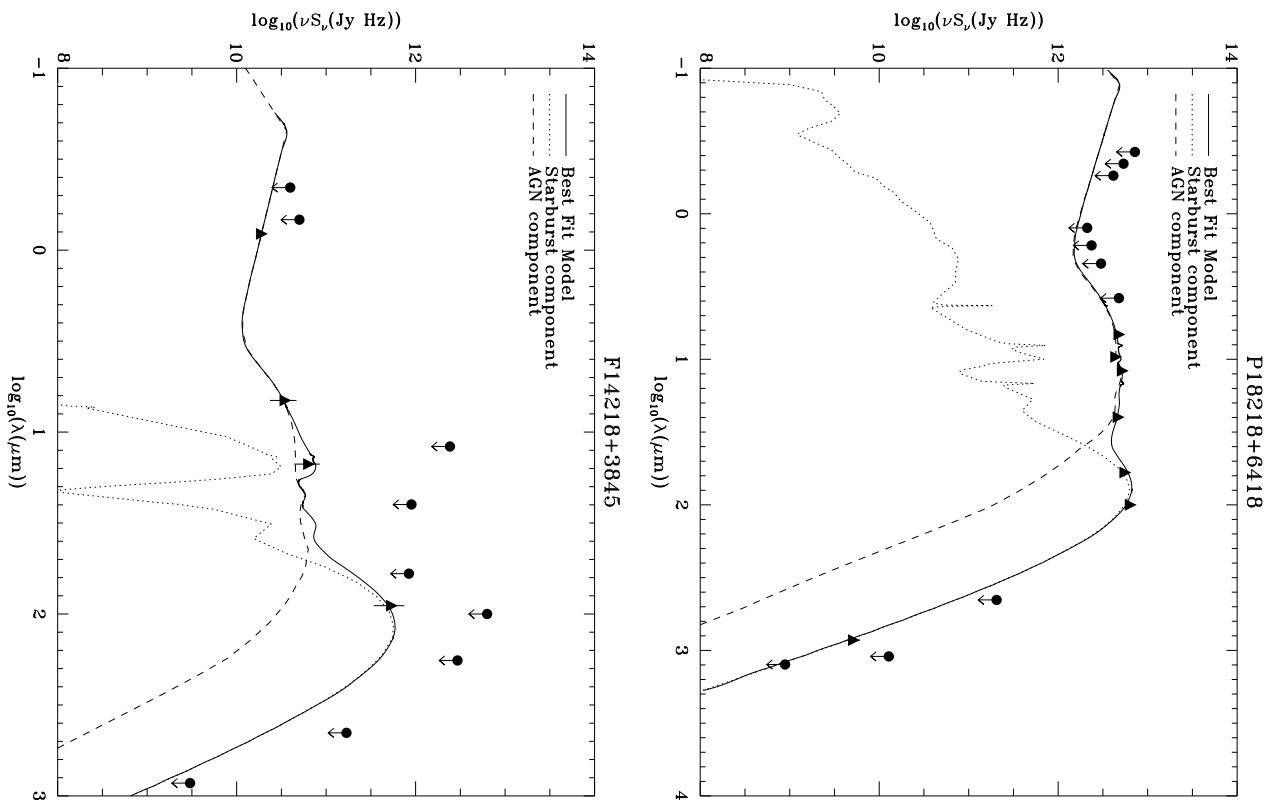


Figure 1 – continued

starburst component dominates, providing 80% of the total IR emission. All the model fits are consistent with a starburst age of $< 57\text{Myr}$, and a dust mass and temperature of $1.07 \times 10^8 M_\odot$ and 45K respectively. The predicted star formation rate is extremely high, at $2000 M_\odot \text{yr}^{-1}$. The best fit SED is presented in Figure 1. The starburst component dominates at rest-frame wavelengths $> 45\mu\text{m}$, with the AGN component dominating in the optical.

4.4.8 IRAS F16124+3241

This object shows no detectable polarized broad lines in the optical, suggesting that the IR emission may be powered by a young starburst rather than a dust shrouded AGN (Tran et al. 1999). With only three fluxes, it is not possible to draw constraints on all model parameters. The best fit total IR luminosity is $\sim 1.1 \times 10^{13} L_\odot$, with the starburst providing $\sim 60\%$ of the IR emission. An AGN component is however required to explain the total IR emission over $1 - 1000\mu\text{m}$.

4.4.9 ELAIS J1640+41

This radio quiet QSO was discovered (Morel et al. 2001) as part of the ELAIS survey (Oliver et al. 2000). Unlike many other HLIRGs this object is detected in the soft X-ray, suggesting that this object may represent the face on analogues of narrow-line HLIRGs (Morel et al. 2001).

A SED fit for this object has been previously presented by Morel et al. (2001). Here we refit the SED with improved

estimates for the *IRAS* upper limits using the SCANPI software. We derive a total IR luminosity of $7.9 \times 10^{12} L_\odot$ with the AGN providing $\sim 70\%$ of the IR emission. The star formation rate is $550 M_\odot \text{yr}^{-1}$. These results are in agreement with Morel et al.

4.4.10 IRAS 18216+6418

This broad line object possesses some enigmatic properties. Radio observations classify it as radio quiet, although the richness of the environment (Abell class ~ 2) is more typical of Radio Loud objects (Lacy, Rawlings & Hill 1992). Many other properties of the system are more typically found in radio loud objects. The host galaxy, with a magnitude of $M_V = -23.2$, is a large, luminous elliptical with no signs of ongoing interaction. The QSO nucleus is slightly offset from the centre of the host galaxy. Radio mapping of this sources show a core and a pair of antipodean jets (Lacy, Rawlings & Hill 1992; Blundell et al. 1996), a radio structure more typically found in RLQs. The radio structure implies that a central supermassive black hole is responsible for the compact radio emission, rather than a starburst (Blundell et al. 1996). Off-nuclear optical spectroscopy shows a spectrum more typically found in radio loud objects (Fried 1998).

In addition to our observations of the QSO we also observed with SCUBA the other object within the *IRAS* error ellipse and found no detection, further supporting the identification of the QSO as the source of the *IRAS* emission. Additional optical photometry for this object was taken

Table 3. Hyperluminous Galaxies: Luminosities and Model Parameters

Name	L_{IR}^{Tot} L_{\odot}	L_{IR}^{Sb} L_{\odot}	L_{IR}^{AGN} L_{\odot}	Age ^a Myr	SFR ^b $M_{\odot}\text{yr}^{-1}$	θ^c °	M_d^d M_{\odot}	T ^e kelvin	β^f
F00235+1024	13.04 ^{+0.08} _{-0.16}	12.74 ^{+0.06} _{-0.20}	12.73 ^{+0.11} _{-0.14}	–	1000 ± 300	< 17.2	8.29 ^{+0.11} _{-0.55}	35 ± 5	1.92 ± 0.1
07380-2342	13.34 ^{+0.01} _{-0.01}	12.85 ^{+0.01} _{-0.03}	13.16 ^{+0.01} _{-0.01}	6.6 – 16	1250 ± 300	< 20	8.79 ^{+0.10} _{-0.21}	31 ± 3	1.97 ± 0.05
F10026+4949	13.81 ^{+0.03} _{-0.13}	13.02 ^{+0.05} _{-0.14}	13.73 ^{+0.03} _{-0.13}	–	2000 ± 600	–	< 8.7	–	–
F12509+3122	13.26 ^{+0.02} _{-0.07}	12.88 ^{+0.09} _{-0.15}	13.02 ^{+0.02} _{-0.07}	–	1050 ± 250	–	8.20 ^{+0.08} _{-0.38}	39 ± 7	1.94 ± 0.07
13279+3401	12.88 ^{+0.10} _{-0.05}	12.39 ^{+0.30} _{-0.37}	12.71 ^{+0.05} _{-0.18}	–	500 ± 300	–	–	–	–
14026+4341	12.90 ^{+0.03} _{-0.50}	12.47 ^{+0.14} _{-0.05}	12.70 ^{+0.03} _{-0.13}	< 57	600 ± 150	–	8.24 ^{+0.05} _{-0.50}	35 ± 5	1.94 ± 0.02
F14218+3845	13.06 ^{+0.02} _{-0.07}	12.96 ^{+0.06} _{-0.17}	12.35 ^{+0.10} _{-0.28}	< 57	2000 ± 500	> 26	8.03 ^{+0.50} _{-0.13}	45 ± 10	1.97 ± 0.02
F16124+3241	13.02 ^{+0.02} _{-0.14}	12.79 ^{+0.07} _{-0.10}	12.63 ^{+0.10} _{-0.35}	–	1100 ± 300	–	8.54 ^{+0.1} _{-0.4}	32 ± 5	1.94 ± 0.05
E J1640+41	12.90 ^{+0.01} _{-0.03}	12.39 ^{+0.09} _{-0.04}	12.73 ^{+0.01} _{-0.04}	–	550 ± 200	–	< 8.2	–	–
18216+6418	13.14 ^{+0.01} _{-0.01}	12.74 ^{+0.02} _{-0.02}	12.91 ^{+0.01} _{-0.01}	26 – 37	1100 ± 200	> 46	8.51 ^{+0.03} _{-0.02}	31 ± 4	1.94 ± 0.01

Luminosities are the logarithm of the 1-1000 μm luminosities obtained from the best fit combined starburst/AGN model, in units of bolometric solar luminosities. ^aStarburst age ^bStar formation rate ^cViewing angle of the AGN dust torus ^dDust mass ^eDust temperature ^fEmissivity index

from Kolman et al. (1993), additional *ISO* fluxes from Clavel et al. (2000), and additional sub-mm data from Andreani, Franceschini & Granato (1999). The comprehensive photometry for this object allows excellent constraints on the best fit model parameters. The best fit total IR luminosity is $1.4 \times 10^{13} L_{\odot}$, with the AGN component providing $\sim 60\%$ of the IR emission. The best fit starburst model parameters are a starburst age of between 26Myr and 37Myr, a dust mass of $3.2 \times 10^8 M_{\odot}$, and a dust temperature of 31K. The inferred star formation rate is $1100 M_{\odot}\text{yr}^{-1}$.

4.4.11 IRAS F23569-0341

Previous *ISO* observations of this object (Verma et al. 2002) did not confirm the *IRAS* 60 μm detection, and did not detect the object in any other band. As we did not detect this source in the sub-mm, its reality remains to be determined. With only one IR flux, it is impossible to draw meaningful constraints on either luminosities or model parameters, we therefore only present a compilation of IR data for this object. Worth noting however is that all the model fits are consistent with a total IR luminosity of $10^{13.5} L_{\odot}$ or less.

5 DISCUSSION

5.1 Starburst & AGN Properties

The contributions from starburst and AGN activity to the total IR emission in the most luminous *IRAS* galaxies has been discussed by several authors. Mid-IR spectroscopy (Genzel et al. 1998; Rigopoulou et al. 1999) found that the IR emission in most ULIRGs ($\sim 80\%$) was powered by starbursts, although at least half of their samples showed evidence for both starburst and AGN activity. There was no detected trend for the AGN-like systems to reside in the more compact (and hence more advanced merger) systems. The fraction of sources powered by an AGN has been shown by several authors to increase with increasing total IR luminosity (Veilleux et al. 1995; Shier, Rieke & Rieke 1996; Veilleux, Sanders & Kim 1999). Recent *ISO* observations of ULIRGs (Tran et al. 2001) found that, at IR luminosities

Table 4. Additional HLIRGs from the literature with calculated starburst and AGN fractions

Name	z	L_{IR}^{Sb} L_{\odot}	L_{IR}^{AGN} L_{\odot}	L_{IR}^{Tot} L_{\odot}
SMMJ02399-0136	2.803	12.89	12.47	13.03
IRAS F10214+4724	2.286	13.10	13.27	13.49
PG1148+549	0.969	13.27	13.51	13.71
IRAS F12514+1027	0.30	12.67	12.63	12.95
H1413+117	2.546	12.71	13.38	13.46
IRAS F14481+4454	0.66	12.94	13.03	13.29
IRAS F15307+3252	0.93	12.96	13.28	13.45

Luminosities are given for $H_0 = 65 \text{ km s}^{-1} \text{ Mpc}^{-1}$, $\Omega_0 = 1.0$.

The luminosities of SMMJ02399-0136, F10214+4724 and H1413+117 have been corrected for the effects of gravitational lensing. Taken from Rowan-Robinson (2000) & Verma et al. (2002).

below $10^{12.4} L_{\odot}$, most ULIRGs were starburst dominated, with the starburst component contributing around 85% to the IR emission. At IR luminosities above $10^{12.4} L_{\odot}$ the AGN contribution was much higher, contributing at least 50% of the IR emission.

Studies of samples of HLIRGs to look for contributions from starbursts and AGN to the total IR emission have yielded interesting results. Studies of small samples of HLIRGs produced conflicting results, with some authors suggesting that the IR emission in HLIRGs arises predominantly from a starburst (Frayer et al. 1998; Frayer et al. 1999) with star formation rates of the order $10^3 M_{\odot}\text{yr}^{-1}$, and other authors suggesting that HLIRGs are powered by a dusty AGN (Granato, Danese & Franceschini 1996; Evans et al. 1998; Yun & Scoville 1998). There is also evidence from spectropolarimetry for a buried AGN in several HLIRGs (Hines et al. 1995; Goodrich et al. 1996) Previous SED modelling of HLIRGs (Rowan-Robinson 2000; Verma et al. 2002) found that most required an AGN and a starburst to power the total IR emission. Overall, about half were AGN dominated. These results were however based on samples either biased toward AGN or lacking the tight constraints on starburst luminosities given by sub-mm data.

The total IR luminosities of the 10 reliably detected objects in our sample, together with the starburst and AGN fractions, are presented in Table 3. In all ten objects both a starburst and an AGN are required to explain the total IR emission; in all cases a ‘pure’ starburst or AGN model is unable to explain the emission over $1 - 1000\mu\text{m}$. The mean starburst fraction in our sample is $\sim 35\%$. In all ten objects both the AGN and starburst components supply at least 20% of the total IR luminosity, any of the objects would be classified as at least a ULIRG with only the starburst or AGN component present. Both starburst and AGN activity in HLIRGs are therefore central in interpreting their properties.

Figure 2 shows a plot of bolometric AGN luminosity plotted against bolometric starburst luminosity for our sample. Also included in this figure are those HLIRGs from Rowan-Robinson (2000) and Verma et al. (2002) that have constrained starburst and AGN fractions. These additional HLIRGs are listed in Table 4. It should be noted that only two of these objects (SMMJ02399-0136 & F10214+4724) are selected in a manner unbiased toward AGN. Three of the objects in Table 4 are gravitationally lensed (SMMJ02399-0136, F10214+4724 & H1413+117), and the effects of lensing must be corrected for to allow comparisons with unlensed objects. For SMMJ02399-0136 we have used the lensed starburst and AGN luminosities given by Rowan-Robinson (2000) and applied a lensing correction of 2.5 (Ivison et al. 1998). For F10214+4724 we have taken the unlensed starburst and AGN luminosities from Green & Rowan-Robinson (1996). For H1413+117 (the ‘Cloverleaf’) we have taken the lensed starburst and AGN luminosities given by Rowan-Robinson (2000) and applied a lensing correction of a factor of 10 (Yun et al. 1997).

It can be seen from Figure 2 that there is a wide spread in fractional power sources across the sample, ranging from 80% starburst dominated to 80% AGN dominated. This is consistent with a similar plot given in Rowan-Robinson (2000) and confirms that a wide spread in fractional starburst luminosities exists over at least 5 orders of magnitude in total IR luminosity in the IR galaxy population. The measured star formation rates are all greater than $500M_{\odot}\text{yr}^{-1}$, and in seven cases exceed $1000M_{\odot}\text{yr}^{-1}$. For the six objects in the sample where the SED shape is constrained, the IR emission longward of $50\mu\text{m}$ in the rest-frame is in all cases dominated by star formation.

Further deductions can be made from Figure 2. With only 5 systems in which the starburst contributes more to the total IR luminosity than the AGN it is impossible to draw conclusions on any correlation between starburst and AGN luminosity. Amongst the 12 AGN dominated systems however there is a strong correlation between the starburst and AGN luminosities. Further comparison with figure 19 from Rowan-Robinson (2000) shows that this correlation extends over 5 orders of magnitude in total IR luminosity. Considering only the AGN dominated HLIRGs in Figure 2, the Spearman rank correlation coefficient between the AGN luminosity and the starburst luminosity is 0.95. When the additional AGN dominated systems from Table 4 are included the correlation coefficient becomes 0.98.

This is an interesting result for understanding AGN and starburst activity in *IRAS* galaxies at all luminosities, as it implies that the luminosities of the AGN and star-

burst components are influenced by common physical factors. On *prima facie* grounds this may seem counterintuitive. Recent studies of starburst and QSO triggering in mergers between gas rich galaxies (Barnes & Hernquist 1996; Taniguchi, Ikeuchi & Shioya 1999; Bekki 2001) suggest a complex pattern of starburst activity. Depending on the impact parameters of the merger, the number of merger progenitors and their morphologies, there may be multiple starburst events triggered throughout the lifetime of the merger. AGN activity conversely, is likely to follow a simpler pattern. If a $> 10^8 M_{\odot}$ black hole is not located in either of the merger progenitors then any central AGN will not reach QSO level luminosities until at least 10^8 years after the merger has commenced (Taniguchi, Ikeuchi & Shioya 1999), leading to a potential lag between any *single* starburst and AGN event. It may thus be expected that there should be at best a weak correlation between starburst or AGN luminosities against total IR luminosities in interaction driven *IRAS* galaxies. Our results however suggest that there is an underlying factor linking the luminosities of the starburst and AGN components. As the physical mechanisms behind star formation and AGN activity are different, the most likely candidate is the available quantity of fuel in the circumnuclear regions of the system. The same reasoning applies if we consider HLIRGs as young galaxies in the process of formation.

The fraction of the IR luminosity due to AGN activity plotted against the total IR luminosity is given in Figure 3. Also plotted are the additional HLIRGs from Table 4. It can be seen that there is no clear trend of increasing AGN fraction with increasing IR luminosity amongst the HLIRG population, irrespective of whether biased or unbiased samples are selected. We therefore find that the trend observed in the ULIRG population of increasing AGN fraction with increasing IR luminosity peaks in the HLIRG population, and that the AGN fraction does not continue to increase at IR luminosities greater than $10^{13}L_{\odot}$.

This study has demonstrated that, to accurately gauge both the total IR luminosity in the most luminous *IRAS* sources, and the contributions from starburst and AGN components, it is necessary to have fluxes and upper limits from the near-IR to the sub-mm. Two objects in our sample (F00235+1024, F14218+3845) have different IR luminosities, and starburst and AGN fractions, than those derived by previous authors (Rowan-Robinson 2000; Verma et al. 2002) without sub-mm fluxes or upper limits.

5.2 Evolutionary Models for HLIRGs

A prevalent picture for the evolution of the most luminous *IRAS* galaxies is the Sanders et al. (1988) picture. Under this picture (hereafter the S88 picture), ULIRGs are the dust shrouded precursors to optical QSOs. Interactions and mergers between gas rich spirals transport gas to the central regions of the galaxies. This large central gas concentration triggers starburst activity, and in the latter stages of the merger commences the fuelling of a central supermassive black hole. In the last stages the dust screen shrouding the black hole is blown away and the ULIRG evolves into an optical QSO. A more recent evolutionary scenario for ULIRGs (Farrah et al. 2001) is that ULIRGs are not a simple precursor stage to optically selected QSOs, but instead are a diverse population whose evolution is driven by the progen-

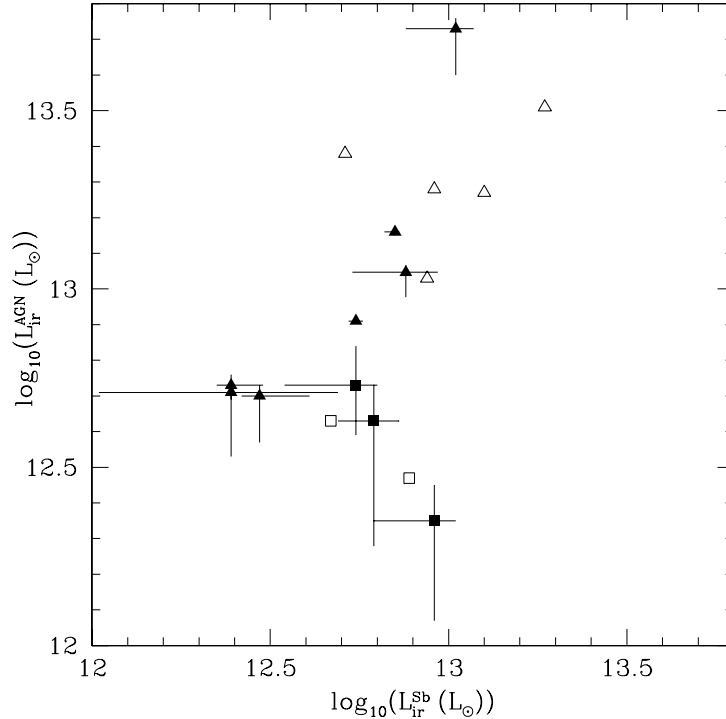


Figure 2. AGN luminosity in the IR plotted against starburst luminosity in the IR. Triangles are AGN dominated systems, squares are Starburst dominated systems. Filled shapes are objects from the sample in this paper, outline shapes are taken from Table 4.

itor morphologies and the local environment. HLIRGs may simply be the high luminosity ‘tail’ of the ULIRG population. Also worth noting is that there is plausible evidence (Farrah et al. 2002) that HLIRGs may lie in very diverse environments, from isolated sources to Abell class ≥ 2 clusters. Such a diversity of environment would give rise to a more diverse range of evolutionary paths.

A recent model for the evolution of HLIRGs in particular is that of Rowan-Robinson (2000). According to this model, HLIRGs are ideal candidates for being ‘primeval’, or very young galaxies, as opposed to mergers between gas rich galaxies. Evidence in support of this is that HLIRGs all have very high star formation rates and a higher gas fraction than typically found in spiral galaxies. The data in this paper, coupled with previous results, allows us to examine whether HLIRGs are very luminous galaxy mergers, or young active galaxies.

The amounts of gas and dust in active galaxies have been examined by several authors and can be a useful diagnostic. In the local Universe, observations of nearby radio galaxies in the sub-mm (Knapp & Patten 1991) found some objects to have comparable dust masses ($\sim 10^7 M_\odot$) to those found in spiral galaxies, but also found other objects with dust masses as low as $\sim 10^4 M_\odot$. At higher redshifts, studies of samples of radio galaxies and radio quiet quasars (Hughes, Dunlop & Rawlings 1997; McMahon et al. 1999; Andreani, Franceschini & Granato 1999) derive dust masses in the range $10^7 < M_{dust}(M_\odot) < 10^9$, with no appreciable dependence on redshift out to $z \sim 5$. These results imply an early accelerated phase of obscured star formation in high redshift primeval galaxies (Franceschini et al. 1994; Mazzei

& de Zotti 1996). Gas and dust masses in HLIRGs have also been the subject of several previous studies, with derived dust masses lying in the range $10^8 < M_{dust}(M_\odot) < 10^9$ (Barvainis, Antonucci & Coleman 1992; Downes, Solomon & Radford 1995; Frayer et al. 1998; Frayer et al. 1999; Verma et al. 2002).

The dust masses derived for the sources in our sample are presented in Table 3. Assuming that the gas to dust ratio in HLIRGs is similar to that in ULIRGs, adopting a gas to dust ratio of 540 (Sanders, Scoville & Soifer 1991) we derive gas masses in the range $10^{10.5} < M_{gas}(M_\odot) < 10^{11.5}$. These gas and dust masses are comparable to those found by previous authors in other HLIRGs, and in other classes of active galaxy. A young, active galaxy may be expected to have both a very high rate of star formation ($\geq 500 M_\odot \text{yr}^{-1}$) in order to form the bulk of its’ stars in ~ 1 Gyr, and a large gas reservoir ($M_{gas} \sim 10^{11} M_\odot$) to maintain this rate of star formation. Both these criteria are satisfied by all the objects in our sample. In addition, several of the host galaxies in our sample show both an elliptical morphology and no signatures of ongoing interaction found in mergers between equal mass spiral galaxies (Farrah et al. 2002). They are therefore excellent candidates for young, active galaxies.

Some of our sample however have optical morphologies that do not fit with this scheme. *HST* imaging (Farrah et al. 2002) has shown that some HLIRGs, such as F00235+1024 and F10026+4949 lie in interacting systems with similar morphologies to local ULIRGs. The most natural interpretation of these sources is that they are the high luminosity ‘tail’ of the ULIRG population. It is also conceivable that the starburst and AGN activity in the dynamically re-

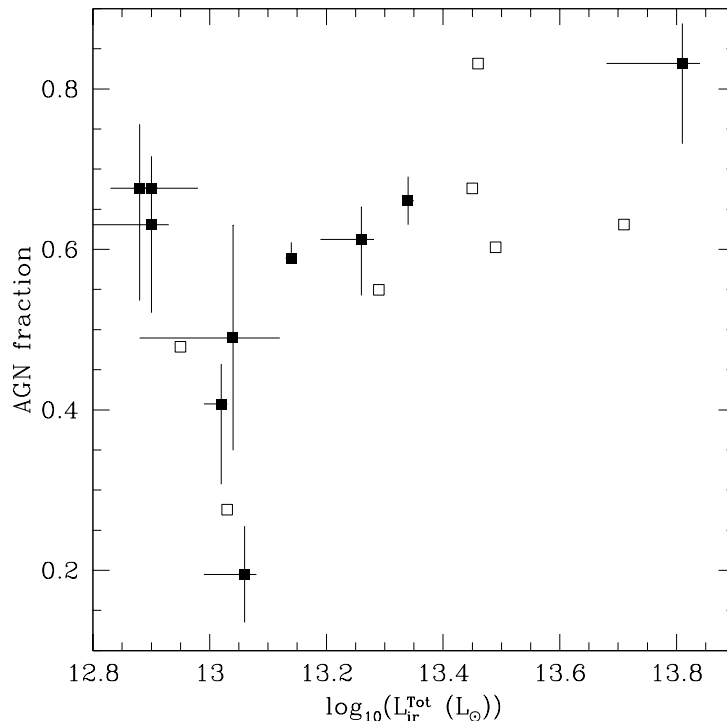


Figure 3. Fraction of the IR luminosity due to AGN activity against the total IR luminosity. Filled squares are objects from this sample, outline squares are the additional HLIRGs from Table 4.

laxed systems in our sample are also triggered by galaxy interactions. The dynamical relaxation time of a merger between galaxies of comparable size is of the order $\sim 10^9$ years (Barnes & Hernquist 1996; Dubinski, Mihos & Hernquist 1999), whereas the lifetime of a QSO (Rees 1984; Martini & Weinberg 2000) and a starburst (Genzel et al. 1998; Thornley et al. 2000) is thought to be no more than $10^{8.5}$ years. It is therefore just possible that a merger driven coeval starburst and AGN could be observed in a dynamically relaxed host, if the starburst and AGN activity were not triggered at or near the start of the merger. More likely though is that the objects in question are very young galaxies going through their maximal star forming period. We therefore conclude that the HLIRG population is comprised of both the most luminous end of the merger driven ULIRG population, and of a population of young active galaxies going through their maximal star formation periods.

5.3 The Cosmic X-ray and Sub-mm Backgrounds

The first three HLIRGs to be discovered were all shown to harbour obscured AGN (Hines et al. 1995). Just as Seyfert 2 galaxies have been suggested to be Seyfert 1 galaxies viewed along a line of sight where the central regions are obscured by dusty tori, HLIRGs have been proposed as ‘misdirected’ QSOs, or QSO-2’s (Hines 1998). A similar picture has also been proposed for radio galaxies (Alighieri, Cimatti & Fosbury 1994). Under this picture, HLIRGs would be classified as Hyperluminous quasars if viewed along a polar line of sight, and as Hyperluminous Galaxies if viewed under any other orientation.

We have shown that all the sources in our sample require extremely luminous AGN to explain the total IR emission. Two objects, IRAS 18216+6418 and ELAIS J1640+41, were previously known to harbour AGN, since they are both luminous in the hard X-ray (Pravdo & Marshall 1984; Morel et al. 2001). On the other hand, deep X-ray observations of 5 other HLIRGs (Fabian et al. 1996; Wilman et al. 1998), including one (F00235+1024) from our sample, did not detect any of the objects, from which it was concluded that these objects were either atypically weak in the X-ray or that the central regions were obscured by columns $N_H > 10^{23} \text{ cm}^{-2}$. From the dust masses and AGN IR luminosities presented in this paper the latter conclusion is preferred. As the sample selection for our study is independent of AGN content, it seems likely therefore that many HLIRGs as a class contain a luminous AGN that is heavily obscured and can only be detected in the IR.

The presence of highly obscured AGN in a large fraction of the most luminous *IRAS* galaxies has interesting implications for interpreting observations of the cosmic X-ray and IR backgrounds. Studies have shown that only $\sim 10\%$ of high- z bright sub-mm sources show signs of AGN activity at other wavelengths (Barger et al. 2001; Almaini et al. 2001). Recent surveys have shown that the hard X-ray background is due almost entirely to AGN (Mushotzky et al. 2000), and there exist models for the X-ray background in which low luminosity AGN produce a hard X-ray spectrum via photoelectric absorption from an obscuring starburst (Fabian et al. 1998; Gunn & Shanks 1999). Estimates of the AGN contribution to deep sub-mm surveys and the IR background (Almaini, Lawrence & Boyle 1998) assume that the fractions

Table 5. Predicted HLIRG SCUBA fluxes extrapolated to higher redshifts

Name	z=2.0		z=3.0	
	S_{850}	S_{450}	S_{850}	S_{450}
F00235+1024	5.3	28.0	6.7	21.2
07380-2342	13.1	59.4	15.2	47.5
F12509+3122	3.0	15.3	3.7	14.9
14026+4341	2.9	15.0	3.5	13.4
F14218+3845	5.6	37.0	7.2	38.5
18216+6418	8.0	40.5	9.7	34.7

All fluxes are given in mJy. Predicted fluxes are given only for those 6 sources with constrained SED shapes.

of obscured and unobscured AGN must fit with the observed cosmic X-ray background, and from this estimate that between 10% and 20% of the $850\mu\text{m}$ SCUBA sources at 1mJy, and a similar fraction of the IR/sub-mm background, are due to AGN.

From our results however it is likely that, at least for the rest-frame most IR luminous sub-mm sources, this picture is not true, and that there exists a population of heavily obscured AGN in sources with $L_{\text{ir}} > 10^{12.5} L_{\odot}$. These AGN will contribute negligibly to the cosmic X-ray background. From the SEDs presented in this paper it is apparent that these AGN may supply a significant fraction, possibly up to 50%, of the contribution to the cosmic background radiation at $\lambda_{\text{obs}} \geq 300\mu\text{m}$ from the most luminous sub-mm sources. Worth noting however is that these SEDs also predict that the $850\mu\text{m}$ background from the most luminous sub-mm sources will in all cases be due to star formation, with a negligible AGN contribution.

5.4 Implications for Sub-mm Surveys

5.4.1 Coeval starburst and AGN activity

There exists substantial observational evidence that, at both low and high redshifts, the main episode(s) of star formation in galaxies are linked with QSO activity. At low redshift there is an observed correlation between black hole mass and bulge mass (Magorrian et al. 1998; Kormendy & Gebhart 2001) with a linear scaling between the two quantities (McLure & Dunlop 2002). At high redshift studies of emission and absorption lines in high- z QSOs typically show that they reside in metal rich (at least $1Z_{\odot}$) environments, and that the more luminous objects may be more metal rich (Hamann & Ferland 1999). Sub-mm continuum observations of high- z QSOs generally show the presence of large masses of cold dust (Omont et al. 1996; Benford et al. 1999). This emission from cold dust is generally ascribed to star formation, although QSO activity is also a possibility (Carilli et al. 2000). The high metallicities in these systems is often seen to indicate that the optical QSO occurs after the bulk of star formation has occurred in the system. A recent study of QSOs and their hosts (Granato et al. 2001) proposes that, in an optical QSO, the star formation is effectively at an end as the QSO power and feedback from supernovae combine to blow out any nuclear starburst (Silk & Rees 1998). An optical QSO activity and high star formation rates are thus predicted not to be coeval. A similar study (Archibald et

al. 2001) predicts that, unless a massive ‘seed’ black hole is already present, luminous AGN activity cannot arise until 0.5Gyr after the first stars form. An independent estimate for the formation of a $> 10^8 M_{\odot}$ black hole in non-nucleated sources (Taniguchi, Ikeuchi & Shioya 1999) gives a timescale of 1Gyr. Therefore, this predicts that there is a time lag between the peak in sub-mm luminosity (due to the starburst) and mid-IR luminosity (due to the AGN) of $\sim 10^8$ years. AGN activity is predicted to only occur in the host once $\sim 90\%$ of the stars in the host have formed and the sub-mm luminosity is only $\sim 25\%$ of its peak value. The predictions from Archibald et al. (2001) are that AGN in luminous high- z sub-mm sources are ~ 1000 times less luminous than the most luminous AGN found in other systems.

The results from our study however suggest that, at least for the most luminous IR galaxies, coeval AGN activity and massive starburst activity exist in many sources, including optical QSOs. Three objects in our sample (F12509+3122, F14218+3845 & ELAIS J1640+41) are optical QSOs containing an extremely luminous AGN together with high rates ($> 500 M_{\odot} \text{yr}^{-1}$) of star formation. The computed star formation rates are so high that it is unphysical to argue that they are not at or near the peak rates of star formation in these systems. In addition the strong correlation between the starburst and AGN luminosities in our sample, implying a common factor governing the luminosities, suggests that the starburst and AGN phases cannot be widely separated in time in HLIRGs.

5.4.2 The nature of high- z sub-mm sources

Two SCUBA galaxies have been previously shown to be HLIRGs (Ivison et al. 2000). A sample of HLIRGs with selection unbiased toward AGN allows us to examine what fraction of HLIRGs as a class would be detected by SCUBA surveys if they lay at higher redshifts. Analysis can only be done for those six sources in the sample (Figure 1) with constrained SED shapes. The fluxes predicted to be observed by SCUBA for these sources if the sources lay at $z = 2$ and $z = 3$ are given in Table 5. At these redshifts all the sources would have observed frame $850\mu\text{m}$ and $450\mu\text{m}$ fluxes comparable to the range of $850\mu\text{m}$ and $450\mu\text{m}$ fluxes for sources found in recent sub-mm surveys (Barger et al. 1998; Eales et al. 2000; Scott et al. 2002; Fox et al. 2002). Thus it seems plausible that at least some fraction of the high- z sources found in sub-mm surveys are similar in nature to the galaxy populations found in the HLIRG population, namely a mixture of ULIRG-like galaxy-galaxy mergers and young active galaxies. It is thus plausible from our results that many of the sources discovered in sub-mm surveys harbour both a dusty starburst and a heavily obscured AGN which contribute comparably to the total rest-frame IR emission. Our study has also shown that, at rest-frame wavelengths $\geq 50\mu\text{m}$ the emission from our sample is starburst dominated. It is therefore a safe assumption that high- z surveys sampling rest-frame wavelengths longward of $50\mu\text{m}$ are for all sources sampling the starburst dominated region of the SED.

It is, however, important to note that X-ray observations of HLIRGs and X-ray surveys of high- z sub-mm sources imply that the two populations are not identical, and that there has been evolution between the two epochs. Of the

seven HLIRGs at $z < 1$ that have deep X-ray observations two (E J1640+41 & 18216+6418) are detected, corresponding to a detection fraction of 28%. Conversely, deep Chandra observations of the SCUBA 8mJy survey regions (Almaini et al. 2001) detect only 2/36 sub-mm sources (assuming a detection threshold of 3.5σ for the sub-mm sources), or $\sim 6\%$. When combined with our results this gives rise to two possibilities. The first is that the fraction of sources that contain luminous AGN is comparable at $z \sim 1$ and $z \sim 3$, with a greater mean obscuration level at $z \sim 3$. The second possibility is that the fraction of sources that contain luminous AGN has declined from $z \sim 3$ to $z \sim 1$. Further deep observations of HLIRGs and high- z sub-mm sources in the X-ray and in the IR will be required to differentiate between these two possibilities.

6 SUMMARY

We have presented sub-mm photometry for 11 Hyperluminous Infrared Galaxies selected purely on the basis of their IR emission, and used radiative transfer codes for starbursts and AGN in conjunction with IR photometry from the literature to examine the power source behind the IR emission from 10 of the objects. Our conclusions are:

(1) In all of the sources both a starburst and AGN component are required to explain the total IR emission. The mean starburst fraction is 35%, with a wide range spanning 80% starburst dominated to 80% AGN dominated. In all cases the starburst dominates at rest-frame wavelengths longwards of $50\mu\text{m}$, with associated star formation rates of at least $500M_{\odot}\text{yr}^{-1}$.

(2) The trend of increasing AGN fraction with increasing IR luminosity observed in the ULIRG population is observed to peak in the HLIRG population. The correlation between the starburst and AGN IR luminosities in the AGN dominated systems implies that the luminosities of both starbursts and AGN in HLIRGs are governed by common physical factors, the most plausible of which is the available quantities of gas and dust in the system

(3) Comparisons between the fractional AGN and starburst luminosities, derived dust masses, and previously published HST imaging suggests that the HLIRG population is comprised both of mergers between gas rich galaxies, as found in the ULIRG population, and of young active galaxies going through their maximal star formation periods whilst harbouring an AGN.

(4) The presence of a luminous AGN in all of the objects in our sample, coupled with the non-detection in the X-ray of most HLIRGs, implies that many galaxies with $L_{\text{ir}} > 10^{12.5}L_{\odot}$ harbour a heavily obscured AGN. Although the contribution from these bright sub-mm galaxies to the total cosmic sub-mm background is small, the contribution from heavily obscured AGN in the brightest sub-mm sources to the cosmic background radiation at $\lambda_{\text{obs}} \geq 300\mu\text{m}$ may therefore be higher than estimates based on constraints from the cosmic X-ray background. The $850\mu\text{m}$ background from the most luminous sub-mm sources will however in all cases be dominated by star formation.

(5) The detection of coeval AGN and starburst activity in our sources coupled with the strong correlation between starburst and AGN luminosity implies that, for the most lu-

minous sub-mm sources, star formation does not cease once the source harbours a luminous AGN. We infer that starburst and AGN activity, and the peak starburst and AGN luminosities, can be coeval in active galaxies generally.

(6) When extrapolated to high- z our sources have comparable observed frame sub-mm fluxes to objects found in sub-mm surveys. At least some high- z sub-mm survey sources are therefore likely to be comprised of similar galaxy populations to those found in the HLIRG population, namely galaxy-galaxy mergers and young active galaxies. It is also plausible from these results that high- z sub-mm sources harbour heavily obscured AGN. It should be noted that $\sim 28\%$ of HLIRGs at $z \lesssim 1$ are detected in the X-ray, whereas only $\sim 6\%$ of high- z sub-mm sources are detected in the X-ray. This implies some evolution between the two epochs. Either the mean AGN obscuration level is greater at $z \sim 3$ than at $z \sim 1$, or the fraction of IR-luminous sources at $z \sim 3$ that contain AGN is smaller than that at $z \sim 1$.

7 ACKNOWLEDGMENTS

We would like to thank Euse Archibald for invaluable help at the JCMT, Matthew Fox and Susie Scott for help with the data reduction and analysis, Jose Afonso for helpful discussion, Kate Isaak for performing the January 2001 observations, Belinda Wilkes for supplying unpublished IR photometry for IRAS 14026+4341, and the anonymous referee for very helpful comments.

The JCMT is operated by the Joint Astronomy Centre on behalf of the UK Particle Physics and Astronomy Research Council, The Netherlands Organization for Scientific Research and the Canadian National Research Council. The work presented has made use of the NASA/IPAC Extragalactic Database (NED), which is operated by the Jet Propulsion Laboratory under contract with NASA, and the Digitized Sky Surveys, which were produced at the Space Telescope Science Institute under U.S. Government grant NAG W-2166. The images of these surveys are based on photographic data obtained using the Oschin Schmidt Telescope on Palomar Mountain and the UK Schmidt Telescope. This research has made use of the NASA/IPAC Infrared Science Archive, which is operated by the Jet Propulsion Laboratory, California Institute of Technology, under contract with the National Aeronautics and Space Administration. D.G.F acknowledges the award of tuition fees and maintenance grant provided by the Particle Physics and Astronomy Research Council. This work was in part supported by PPARC (grant number GR/K98728).

REFERENCES

- Alighieri, S. D. S., Cimatti A., Fosbury R. A. E., 1994, ApJ, 431, 123
- Almaini O., Lawrence A., Boyle B. J., 1999, MNRAS, 305L, 59
- Almaini O., et al, MNRAS accepted, astro-ph 0108400
- Andreani P., Franceschini A., Granato G., 1999, MNRAS, 306, 161
- Archibald E. N., Wagg J. W., Jenness T., 2000, SCD System Note 2.2
- Archibald E.N., Dunlop J.S., Jimenez R., Friaca A.C.S., McLure R.J., Hughes D.H., 2001, ApJ Submitted

- Barger A. J., Cowie L. L., Sanders D. B., Fulton E., Taniguchi Y., Sato Y., Kawara K., Okuda H., 1998, *Nat*, 394, 248
- Barger A. J., Cowie L. L., Mushotzky R. F., Richards E. A., 2001, *AJ*, 121, 662
- Barnes J., Hernquist L., 1996, *ApJ*, 471, 115
- Barvainis R., Antonucci R., Coleman P., 1992, *ApJ*, 399L, 19
- Becker R. H., et al, 2001, *AJ Accepted*, astro-ph 0108097
- Bekki K., 2001, *ApJ*, 2001, *ApJ*, 546, 189
- Benford D. J., Cox P., Omont A., Phillips T. G., McMahon R. G., 1999, *ApJ*, 518L, 65
- Blundell K. M., Beasley A. J., Lacy M., Garrington S. T., 1996, *ApJL*, 468L, 91
- Broadhurst T., Lehar J., 1995, *ApJ*, 450L, 41
- Brown R. L., vanden Bout P. A., 1991, *AJ*, 102, 1956
- Bruzual A. G., Charlot S., 1993, *ApJ*, 405, 538
- Carilli C. L., et al, 2000, *ApJ*, 533L, 13
- Clavel J., et al, 2000, *A&A*, 357, 839
- Devereux N. A., Young J. S., 1990, *ApJ*, 359, 42
- Downes D., Solomon P. M., Radford S. J. E., 1995, *ApJ*, 453L, 65
- Dubinski J., Mihos J. C., Hernquist L., 1999, *ApJ*, 526, 607
- Eales S., Lilly S., Webb T., Dunne L., Gear W., Clements D., Yun M., 2000, *AJ*, 120, 2244
- Efstathiou A., Rowan-Robinson M., 1995, *MNRAS*, 273, 649
- Efstathiou A., Rowan-Robinson M., Siebenmorgen R., 2000, *MNRAS*, 313, 734
- Eisenhardt P. R., Armus L., Hogg D. W., Soifer B. T., Neugebauer G., Werner M. W., 1996, *ApJ*, 461, 72
- Elston R., McCarthy P. J., Eisenhardt P., Dickinson M., Spinrad H., Januzzi B. T., Maloney P., 1994, *AJ*, 107, 910
- Evans A. S., Sanders D. B., Cutri R. M., Radford S. J. E., Surace J. A., Solomon P. M., Downes D., Kramer C., 1998, *ApJ*, 506, 205
- Fabian A. C., Cutri R. M., Smith H. E., Crawford C. S., Brandt W. N., 1996, *MNRAS*, 283L, 95
- Fabian A. C., Barcons X., Almaini O., Iwasawa K., 1998, *MNRAS*, 297L, 11
- Farrah D., et al, 2001, *MNRAS*, 326, 1333
- Farrah D., Verma A., Oliver S., Rowan-Robinson M., McMahon R., 2002, *MNRAS*, 329, 605
- Fox M., et al, 2002, *MNRAS*, 331, 839
- Franceschini A., Mazzei P., de Zotti G., Danese L., 1994, *ApJ*, 427, 140
- Frayer D. T., Ivison R. J., Scoville N. Z., Yun M., Evans A. S., Smail I., Blain A. W., Kneib J.-P., 1998, *ApJ*, 506L, 7
- Frayer D. T., et al, 1999, *ApJ*, 514L, 13
- Fried J. W., 1998, *A & A*, 331L, 73
- Genzel R., et al, 1998, *ApJ*, 498, 579
- Goodrich R. W., Miller J. S., Martel A., Cohen M. H., Tran H. D., Ogle P. M., Vermeulen R. C., 1996, *ApJ*, 456L, 9
- Graham J. R., Liu M. C., 1995, *ApJ*, 449L, 29
- Granato G. L., Danese L., Franceschini A., 1996, *ApJ*, 460L, 11
- Granato G. L., Silva L., Monaco P., Panuzzo P., Salucci P., De Zotti G., Danese L., 2001, *MNRAS*, 324, 757
- Green S. M., Rowan-Robinson M., 1996, *MNRAS*, 279, 884
- Gunn K. F., Shanks T., 1999, *MNRAS submitted*, astro-ph 9909089
- Hamann F., Ferland G., 1999, *ARA&A*, 37, 487
- Hildebrand R. H., 1983, *QJRAS*, 24, 267
- Hines D. C., Schmidt G. D., Smith P. S., Cutri R. M., Low F. J., 1995, *ApJ*, 450L, 1
- Hines D. C., 1998, *AAS*, 193, 2704
- Hines D. C., Schmidt G. D., Gordon K. D., Wills B. J., Smith P. S., Allen R. G., Sitko M. L., 2001, *AAS*, 198, 7408
- Holland W. S., et al, 1999, *MNRAS*, 303, 659
- Hughes D. H., Dunlop J. S., Rawlings S., 1997, *MNRAS*, 289, 766
- Hutchings J. B., Neff S.G., 1991, *AJ* 101, 2001
- Hutchings J. B., Morris S. C., 1995, *AJ*, 109, 1541
- Ivison R. J., Smail I., Le Borgne J.-F., Blain A. W., Kneib J.-P., Bezecourt J., Kerr T. H., Davies J. K., 1998, *MNRAS*, 298, 583
- Ivison R. J., Smail I., Barger A. J., Kneib J.-P., Blain A. W., Owen F. N., Kerr T. H., Cowie L. L., 2000, *MNRAS*, 315, 209
- Kleinmann S. G., Hamilton D., Keel W. C., Wynn-Williams C. G., Eales S. A., Becklin E. E., Kuntz K. D., 1988, *ApJ*, 328, 161
- Knapp G. R., Patten B. M., 1991, *AJ*, 101, 1609
- Kolman M., Halpern J. P., Shrader C. R., Filippenko A. V., Fink H. H., Schaeidt S. G., 1993, *ApJ*, 402, 514
- Kormendy J., Gebhart K., 2001, 20th Texas Symposium on Relativistic Astrophysics, ed. H. Martel & J.C. Wheeler, AIP, in press
- Lacy M., Rawlings S., Hill G.J., 1992, *MNRAS* 258, 828
- Lawrence A., et al, 1993, *MNRAS*, 260, 28
- Low F. J., Cutri R. M., Kleinmann S. G., Huchra J. P., 1989, *ApJ*, 340L, 1
- Magorrian J., et al, 1998, *AJ*, 115, 2285
- Martini P., Weinberg D. H., 2001, *ApJ*, 547, 12
- Mazzei P., de Zotti G., 1996, *MNRAS*, 279, 535
- McLure R. J., Dunlop J. S., 2002, *MNRAS*, 331, 795
- McMahon R. G., Priddey R. S., Omont A., Snellen I., Withington S., 1999, *MNRAS*, 309L, 1
- Morel T., et al, 2001, *MNRAS*, 327, 1187
- Moshir M., et al, 1992, *IRAS Faint Source Catalogue*, version 2.0
- Mushotzky R. F., Cowie L. L., Barger A. J., Arnaud K. A., 2000, *Nat*, 404, 459
- Oliver S., et al, 2000, *MNRAS*, 316, 749
- Omont A., McMahon R. G., Cox P., Kreysa E., Bergeron J., Pajot F., Storrie-Lombardi L. J., 1996, *A&A*, 315, 10
- Pravdo S. H., Marshall F. E., 1984, *ApJ*, 281, 570
- Rigopoulou D., Spoon H. W. W., Genzel R., Lutz D., Moorwood A. F. M., Tran Q. D., 1999, *AJ*, 118, 2625
- Rees M. J., *ARA&A*, 22, 471
- Rowan-Robinson M., et al, 1991, *Nat.*, 351, 719
- Rowan-Robinson M., 1992, *MNRAS*, 258, 787
- Rowan-Robinson M., 1995, *MNRAS*, 272, 737
- Rowan-Robinson M., et al, 1997, *MNRAS*, 289, 490
- Rowan-Robinson M., 2000, *MNRAS*, 316, 885
- Sanders D. B., Soifer B. T., Elias J. H., Madore B. F., Matthews K., Neugebauer G., Scoville N. Z., 1988, *ApJ*, 325, 74
- Sanders D. B., Scoville N. Z., Soifer B. T., 1991, *ApJ*, 370, 158
- Sanders D. B., Mirabel I. F., 1996, *ARA&A*, 34, 749-792
- Scott S. E., et al, 2002, *MNRAS*, 331, 817
- Shier L. M., Rieke M. J., Rieke G. H., 1996, *ApJ*, 470, 222
- Siebenmorgen R., Krugel E., 1992, *A&A*, 259, 614
- Silk J., Rees M. J., 1998, *A&A*, 331L, 1
- Soifer B. T., et al, 1984, *ApJ*, 278L, 71
- Soifer B. T., Neugebauer G., Matthews K., Armus L., 1994, *ApJ*, 433L, 69
- Solomon P. M., Downes D., Radford S. J. E., 1992, *ApJ*, 398L, 29
- Taniguchi Y., Ikeuchi S., Shioya Y., 1999, *ApJ*, 514L, 9
- Thornley M. D., Schreiber N. M., Forster L. D., Genzel R., Spoon H. W. W., Kunze D., Sternberg A., 2000, *ApJ*, 539, 641
- Tran H. D., Brotherton M. S., Stanford S. A., van Breugel W., Dey A., Stern D., Antonucci R., 1999, *ApJ*, 516, 85
- Tran Q. D., et al, 2001, *ApJ*, 552, 527
- Veilleux S., Kim D.-C., Sanders D. B., Mazzarella J. M., Soifer B. T., 1995, *ApJS*, 98, 171
- Veilleux S., Sanders D. B., Kim D.-C., 1999, *ApJ*, 522, 139
- Verma A., Rowan-Robinson M., McMahon R., Efstathiou A., 2002, *MNRAS*, Submitted
- Wiklund T., Henkel C., 1995, *A&A*, 297, L71
- Wilman R. J., Fabian A. C., Cutri R. M., Crawford C. S., Brandt W. N., 1998, *MNRAS*, 300L, 7

Yun M. S., Scoville N. Z., Carrasco J. J., Blandford R. D., 1997,
ApJ, 479L, 9
Yun M. S., Scoville N. Z., 1998, ApJ, 507, 774

This paper has been produced using the Royal Astronomical
Society/Blackwell Science \LaTeX style file.